MSc in Photonics

PHOTONICS**BCN**

Universitat Politècnica de Catalunya (UPC)
Universitat Autònoma de Barcelona (UAB)
Universitat de Barcelona (UB)
Institut de Ciències Fotòniques (ICFO)

http://www.photonicsbcn.eu

Master in Photonics

MASTER THESIS WORK

TWISTED ELECTRONS AS AN IMAGING TOOL FOR PROBING CHIRAL MOLECULES IN STRONG FIELD IONIZATION

Xavier Barcons Planas

Supervised by Prof. Dr. Maciej Lewenstein, (ICFO)

Co-supervised by Dr. Andrew Maxwell and Dr. Andrés Ordoñez, (ICFO)

Presented on date 8th September 2021

Registered at

Escola Tècnica Superior d'Enginyeria de Telecomunicació de Barcelona

Twisted electrons as an imaging tool for probing chiral molecules in strong field ionization

Xavier Barcons Planas

ICFO - Institut de Ciències Fotòniques, The Barcelona Institute of Science and Technology, 08860 Castelldefels (Barcelona), Spain

E-mail: xavierbarconsplanas@gmail.com

August 2021

Abstract. Orbital angular momentum (OAM) carried by vortex beams has seen an explosion of interest across fields and this is particularly true in attosecond physics. Given that twisted electrons have been shown to be sensitive to the chirality of molecules, exploring this sensitivity on the attosecond scale is a particularly exciting prospect. The OAM of photoelectrons has been theoretically studied discussing ways to measure and understand the ionization via an analytic formalism. This opens up the possibility of using the photoelectron OAM as an imaging tool. However, in most of the earlier studies the effects of the initial state on the photoelectron OAM have been neglected. In this project, using an analytic formalism to produce chiral hydrogen states, we have investigated how the photoelectron OAM in strong field ionization can be used to image molecular chirality.

Keywords: strong-field physics, ionization, electron vortices, orbital angular momentum, chirality

1. Introduction

The wave-particle duality of free electrons manifests itself naturally in some processes. Concretely, the electron's wave nature can be revealed in the phase acquired upon propagation. In problems without external potentials, a typical solution of the wave (Schrödinger) equation is a structured wave, a superposition of multiple plane waves which interference results in phase singularities. Such structured waves are called vortices due to a swirl in the probability current density around the phase singularities, so they possess angular-momentum properties. Therefore, a vortex beam is a freely propagating beam of particles having well-defined orbital angular momentum (OAM) about its propagation axis [1]. The majority of studies on vortex beams dealt with optical and classical fields, but the similarities between electron optics and photonics suggested the application of the results also to electrons. Electron vortex beams have a wide range of applications in various fields [2], such as high-energy physics, electron microscopy or fundamentals of quantum mechanics.

Electron vortex beams have been proposed to characterize the optical response of chiral structures [3], demonstrating the chiral exchange of OAM and a high degree of dichroism between a vortex electron beam and a chiral sample.

Chiral objects, structures with broken mirror symmetry, are very abundant in nature, ranging from fundamental particles to spiral galaxies. A chiral object and its mirror image, like a left hand and a right hand, constitute a pair of enantiomers. At the molecular level, a specific chirality is crucial for encoding genetic information. Most substances relevant to biology (amino acids, carbohydrates, nucleic acids...) have a certain chirality and, although the homochirality of life is recognised [4], it is not yet understood despite the every-day implications that has on living organisms at the molecular level. Furthermore, chirality has a huge impact in pharmaceutical products [5], a market where half of the drugs are chiral. Therefore, the investigation of techniques for probing molecular chirality and distinguishing enantiomers is an attractive topic.

Molecular chirality can be probed using light, by studying the interaction between chiral molecules and an electromagnetic field. The photoelectrons ejected on absorption of circularly polarized light by a sample of randomly oriented molecules have an angular distribution [6], which for chiral molecules displays a forward-backward asymmetry referred to as photoelectron circular dichroism (PECD) [7]. PECD is one of the most sensitive probes of molecular chirality, since the chiral effects still occur within the electric-dipole approximation, in contrast to standard methods such as absorption circular dichroism or optical rotation. It has been experimentally demonstrated that PECD exists in the strong-field regime [8].

With the advances in laser technology, few-cycle femtosecond laser pulses became routinely available, permitting the study of the atomic-scale motion of electrons [9]. Although the interaction of a weak laser field with an atom or a molecule can be completely understood by the conventional perturbation theory, this is no longer applicable in the strong field case. An alternative perturbation theory, the strong field approximation (SFA) [10, 11], includes the exact laser field and treats the field-free system potential as a perturbation. The SFA is an analytical approximation method to solve the time-dependent Schrödinger equation and, consequently, to understand and describe atomic or molecular dynamics in strong laser fields. This theory, pioneered by Keldysh, Reiss and Faisal [12, 13, 14], opened up a rich set of physical phenomena associated with attosecond science. A laser pulse can promote an electron into the continuum (see [15] for a review of the theoretical description), and the quantum interference patterns present in the strong field phenomena of one or two ionization processes are explored at [16]. The study of the OAM of photoelectrons has been used to measure and understand the ionization via an analytical formalism [17]. Furthermore, the conservation laws for the angular momenta of twisted electrons in strong field ionization have been derived for different polarised fields [18]. Given that vortex electrons have been shown to be sensitive to the target structure [19], the photoelectron OAM can be used as an imaging tool.

In this work, we want to investigate how molecular chirality is imprinted on the vortex beams in strong field ionization. We utilize the strong field approximation to describe the ionization dynamics of chiral wave functions resulting from superpositions of hydrogen states [20]. We have shown, theoretically, that an electron ionized by a linearly polarized laser field from a wave function constituted by superpositions of hydrogen states has the same OAM values as the magnetic quantum numbers of the hydrogen states. Furthermore, we exploit this to demonstrate that the two opposite enantiomers have asymmetric OAM distributions, a phenomenon we have called photoelectron vortex dichroism that can be experimentally implemented to probe chiral molecules and distinguish enantiomers.

The present project is organized as follows. Sec. 2 introduces the theoretical framework: the scattering matrix formalism and the strong field approximation, as well as the theory of electron vortex beams and the ionization of chiral molecules. Sec. 3 presents the results, and the conclusions are analyzed in Sec. 4. The work presented in Sec. 3 is new and my own.

2. Background

2.1. Scattering matrix and Strong Field Approximation

In this section we develop the scattering matrix formalism and SFA. Throughout the thesis we used atomic units (a.u.) i.e. $\hbar = m_e = e = 1$, where $\hbar$ is the reduced Planck's constant, m_e is the mass of the electron and e is the elementary charge. The charge of the electron in these units is -1.

The evolution of an electron under the influence of a binding potential and a strong laser field is described by the time-dependent Schrödinger equation

$$\hat{H}(t)\,|\psi(t)\rangle = i\frac{\partial}{\partial t}\,|\psi(t)\rangle\,, \tag{1}$$

with Hamiltonian

$$\hat{H}^{(c)}(t) = \frac{1}{2}\left(\hat{\mathbf{p}} + \mathbf{A}(t)\right)^2 + V(\hat{\mathbf{r}}) \tag{2}$$

in the velocity (Coulomb) gauge (gauge fixing condition $\nabla \cdot \mathbf{A} = 0$). Here $V(\hat{\mathbf{r}})$ is the Coulomb potential, $\hat{\mathbf{p}}$ the momentum operator and $\mathbf{A}(t)$ the classical vector potential, in which the dipole approximation, $\mathbf{A}(\hat{\mathbf{r}}, t) \approx \mathbf{A}(t)$, is considered since the wavelength of the field is much larger than the size of the system.

The Hamiltonian can be split into $\hat{H}(t) = \hat{H}_a + \hat{H}_I(t)$, where $\hat{H}_a = \hat{\mathbf{p}}^2/2 + V(\hat{\mathbf{r}})$ is the field-free Hamiltonian and $\hat{H}_I(t) = \hat{\mathbf{p}} \cdot \mathbf{A}(t) + \mathbf{A}^2(t)/2$ the electron-field interaction Hamiltonian.

In the length gauge, the Hamiltonian is

$$\hat{H}^{(l)}(t) = \frac{1}{2}\hat{\mathbf{p}}^2 + \hat{\mathbf{r}} \cdot \mathbf{E}(t) + V(\hat{\mathbf{r}}), \tag{3}$$

where $\mathbf{E}(t)$ is the electric field of the laser in the dipole approximation and the interaction of the electron with that field is given by $\hat{H}_I(t) = \hat{\mathbf{r}} \cdot \mathbf{E}(t)$. Although quantum mechanics is gauge invariant, due to approximation this is not the case for the SFA [21].

The previous equation can not be solved analytically. Nevertheless, the dynamics of the system can be probed by writing the problem as a scattering matrix transition amplitude. The transition amplitude of an ionizing electron can be written as

$$M_f = \lim_{\substack{t\to\infty \\ t_0\to-\infty}} \langle \psi_f(t)| \, U(t,t_0) \, |\psi(t_0)\rangle \,, \tag{4}$$

being $|\psi_f(t)\rangle$ the final unbound state and $|\psi(t_0)\rangle$ the initial field-free bound state. The time evolution operator $U(t,t_0)$ can be written using the Dyson equation:

$$U(t,t_0) = U_a(t,t_0) - i\int_{t_0}^{t} U(t,t')H_I(t')U_a(t',t_0)dt', \tag{5}$$

where $U_a(t,t_0)$ is the time-evolution operator for the field-free Hamiltonian.

Substituting $U(t,t_0)$ into the S-matrix transition amplitude leads to the formally exact ionization amplitude [22]

$$M_f = -i \lim_{t\to\infty} \int_{-\infty}^{t} dt' \, \langle \psi_f(t)| \, U(t,t')H_I(t') \, |\psi_0(t')\rangle \,, \tag{6}$$

with $|\psi_0(t')\rangle = e^{iI_p t'} \, |\psi_0\rangle$, being I_p the ionization potential.

In the strong field approximation, the Coulomb potential is neglected for electrons in the continuum. Therefore, the time evolution operator $U(t,t')$, upon neglection of continuum-continuum matrix elements responsible for rescattering [23], reduces to the Volkov operator $U_v(t,t')$, given by

$$U_v(t,t') = \int d^3\mathbf{p} \, e^{-\frac{i}{2}\int_{t'}^{t} d\tau(\mathbf{p}+\mathbf{A}(\tau))^2} \, |\tilde{\mathbf{p}}(t)\rangle \, \langle \tilde{\mathbf{p}}(t')| \,, \tag{7}$$

where $\tilde{\mathbf{p}}(t) = \mathbf{p}$ in the velocity gauge and $\tilde{\mathbf{p}}(t) = \mathbf{p} + \mathbf{A}(t)$ in the length gauge.

Assuming that at $t \to \infty$ the electric field is 0 i.e. $\mathbf{A}(t) = 0$, we get the following expression for the transition amplitude:

$$M_f = -i \lim_{t\to\infty} \int_{-\infty}^{t} dt' \int d^3\mathbf{p}' e^{-iS(\mathbf{p}',t)} \, \langle \psi_f| \, \mathbf{p}'\rangle d(\mathbf{p}',t') e^{iS(\mathbf{p}',t')}, \tag{8}$$

where the exponential terms from the continuum evolution and bound state evolution are collected together into a quasi-classical action,

$$S(\mathbf{p},t) = I_p t + \frac{1}{2}\int_{-\infty}^{t} d\tau(\mathbf{p} + \mathbf{A}(\tau))^2, \tag{9}$$

which describes the propagation of an electron from the ionization time to the end of the pulse. Furthermore, the information about the interaction and electronic bound state is considered in the prefactor

$$d(\mathbf{p},t') = \langle \tilde{\mathbf{p}}(t')| \, V(\hat{\mathbf{r}}) \, |\psi_0\rangle \,, \tag{10}$$

in which we have replaced $\hat{H}_I$ by $V(\hat{\mathbf{r}})$ due to orthogonal relations of the inner product [24].

For a plane wave momentum state as the final continuum state, $\langle \psi_f| \, \mathbf{p}'\rangle \to \langle \mathbf{p}| \, \mathbf{p}'\rangle = \delta(\mathbf{p}' - \mathbf{p})$ and therefore

$$M_f \to M(\mathbf{p}) = -i\int_{-\infty}^{+\infty} dt' d(\mathbf{p},t') e^{iS(\mathbf{p},t')}. \tag{11}$$

The previous plane-wave transition amplitude can be computed using the saddle point approximation [25], a method for approximating integrals, as

$$M(\mathbf{p}) \approx \sum_{t_s} \sqrt{\frac{2\pi i}{S''(\mathbf{p}, t_s)}} d(\mathbf{p}, t_s) e^{iS(\mathbf{p}, t_s)}, \tag{12}$$

where t_s are the times that cancel the first derivative of the action ($S'(\mathbf{p}, t_s) = 0$) given by

$$(\mathbf{p} + \mathbf{A}(t_s))^2 = -2I_p. \tag{13}$$

These times will be complex due to the non-classical nature of tunneling.

2.2. Vortex states

Electron vortex beams are freely propagating vortex states having well-defined OAM about their propagation axis, with a wavefront with quantized topological structure arising from a singularity in phase $e^{il\phi}$, with ϕ the azimuthal angle about the beam axis and l the topological charge with integer value known as the orbital angular momentum. The general form of a Bessel beam electron-vortex state is

$$\psi_l(\mathbf{r}, t) = \langle \mathbf{r} | \, \psi_l(t) \rangle = N_l J_l(p_\perp r_\perp) e^{il\phi} e^{ip_\parallel r_\parallel} e^{-i\omega t}, \tag{14}$$

where N_l is a normalization factor and $J_l(p_\perp r_\perp)$ is the Bessel function of the first kind, being $(p_\parallel, p_\perp, \phi)$ the cylindrical coordinates of $\mathbf{p}$. The Fourier transform, ignoring the time dependence and the normalization factor, is

$$\langle \mathbf{p}' | \, \psi_l(t) \rangle = \frac{i^{-l} e^{il\phi'}}{2\pi p_\perp} \delta(p'_\parallel - p_\parallel) \delta(p'_\perp - p_\perp). \tag{15}$$

Therefore, if a Bessel beam vortex state is used as final continuum state, the transition amplitude reads

$$M_l(p_\parallel, p_\perp) = \frac{i^l}{2\pi} \int_{-\pi}^{\pi} d\phi \, e^{-iS(\mathbf{p}, t)} e^{-il\phi} M(\mathbf{p}). \tag{16}$$

2.3. Ionization of chiral molecules

The photoelectron momentum distribution formed by vortex electrons is expected to be sensitive to the chirality (handedness) of the initial state. A molecule is said to be chiral if it cannot be superposed on its mirror image by any combination of rotations and translations. A chiral molecule and its mirror image, which have different handedness, are called enantiomers.

Nevertheless, calculations with molecules are more time-consuming. As a first step towards gaining insight about the emergence of OAM in the strong field ionization of chiral molecules, chiral hydrogen states can be used, thus getting simpler analytical results. These states capture the chirality of the ground state, have been used to analyse PECD, and can be readily implemented in the current atomic code.

Among the different types of hydrogen chiral wave functions, an interesting one is the ρ-type state [20]

$$|\chi_\rho^\pm\rangle = \frac{1}{2}(|4d_{\pm1}\rangle + i\,|4f_{\pm1}\rangle - |4d_{\mp1}\rangle + i\,|4f_{\mp1}\rangle), \tag{17}$$

where $|n\ell_m\rangle$ denotes the hydrogenic state with n, ℓ and m principal, orbital and magnetic quantum number, respectively. $|\chi_\rho^+\rangle$ and $|\chi_\rho^-\rangle$ are the two enantiomers, related to each other through a reflection. The wave function can be written as $|\chi_\rho^\pm\rangle = (|\chi_c^\pm\rangle + |\chi_c^\pm\rangle^*)/\sqrt{2}$, being $|\chi_c^\pm\rangle = (|4d_{\pm1}\rangle + i\,|4f_{\pm1}\rangle)/\sqrt{2}$ the c-type hydrogen wave function. The enantiomers $\chi_\rho(\mathbf{r})$ are shown in Fig. 1. The ρ-type wave function is particularly meaningful because it has a chiral probability density and, therefore, it mimics the electronic ground state of an actual chiral molecule.

The ionization with circularly polarized light of chiral molecules results in PECD, which manifests in forward-backward asymmetry in the photoelectron angular distribution. This is a very sensitive probe of photoionization dynamics and of molecular structure, because unlike optical activity and absorption, circular dichroism occurs within the electric-dipole approximation. In this project, following the idea of PECD, we will study the ionization of the ρ-type wave function with linearly polarized light.

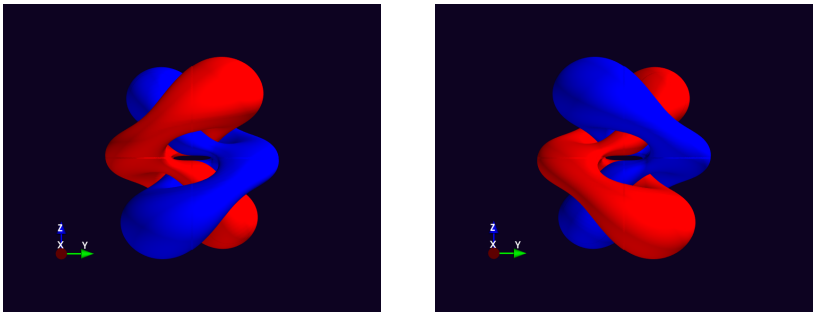

Figure 1: Positive (blue) and negative (red) isosurfaces $\chi_\rho^+(\mathbf{r}) = \pm 0.003$ a.u. (left) and $\chi_\rho^-(\mathbf{r}) = \pm 0.003$ a.u. (right).

2.4. The prefactor

The prefactor related to the ionization of the electron is

$$d(\mathbf{p}, t') = \langle \tilde{\mathbf{p}}(t') | \, V(\hat{\mathbf{r}}) \, | \psi_g \rangle = \frac{1}{(2\pi)^{3/2}} \int d^3 r V(\mathbf{r}) e^{-i\tilde{\mathbf{p}}\cdot\mathbf{r}} \psi_g(\mathbf{r}), \tag{18}$$

where $\tilde{\mathbf{p}}(t') = \mathbf{p}$ in the velocity gauge and $\tilde{\mathbf{p}}(t') = \mathbf{p} + \mathbf{A}(t')$ in the length gauge. For a hydrogenic state, $\psi_g(\mathbf{r}) = R_{n\ell}(r) Y_\ell^m(\theta, \phi)$, where $R_{n\ell}$ is the radial part of the wave function and Y_ℓ^m the spherical harmonic, and $V(\mathbf{r}) = -1/r$ is the binding potential. Furthermore, the plane wave can be expanded into spherical harmonics as

$$e^{-i\mathbf{p}\cdot\mathbf{r}} = 4\pi \sum_{\ell=0}^{\infty} (-i)^\ell j_\ell(pr) \sum_{m=-\ell}^{\ell} \bar{Y}_\ell^m(\theta_r, \phi_r) Y_\ell^m(\theta_p, \phi_p), \tag{19}$$

being j_ℓ the spherical Bessel functions.

Writing $R_{n\ell}(r)$ as a sum of associated Laguerre polynomials and doing some integrals (see [26]), finally we get

$$\begin{aligned} d(\mathbf{p}, t') = (-i)^\ell \sqrt{\frac{(n-\ell-1)!}{2n\,(n+\ell)!}} Y_\ell^m(\theta_{\tilde{p}}, \phi_{\tilde{p}}) \sum_{k=0}^{n-\ell-1} \frac{(n+\ell)! \left(\sqrt{2I_p}\right)^{-\frac{1}{2}-\ell} \left(\tilde{\mathbf{p}}^2(t')\right)^{\ell/2}}{\Gamma\left(\frac{3}{2}+\ell\right)(n-\ell-k-1)!k!} \\ \times (-2)^k \; {}_2F_1\left(\frac{1}{2}(2+k+2\ell), \frac{1}{2}(3+k+2\ell); \frac{3}{2}+\ell; -\frac{\tilde{\mathbf{p}}^2(t')}{2I_p}\right), \end{aligned} \tag{20}$$

where ${}_2F_1(a, b; c; z)$ is the ordinary hypergeometric function.

Besides, if $|\psi_g\rangle = \sum_i |\psi_g^i\rangle$, $d(\mathbf{p}, t') = \sum_i d_i(\mathbf{p}, t')$, where $d_i(\mathbf{p}, t') = \langle \tilde{\mathbf{p}}(t') | \, V(\hat{\mathbf{r}}) \, | \psi_g^i \rangle$.

3. Results

In this section we will examine the electron's momentum and OAM distributions for different initial states.

We will employ a laser field with 12-cycle laser pulses linearly polarized along the z axis. The field's vector potential can be written as

$$\mathbf{A}(t) = A_0 \sin\left(\frac{\omega t}{2N}\right)^2 \cos(\omega t + \delta)\, \mathbf{e}_z, \tag{21}$$

being $A_0 = 2\sqrt{U_p}$ the peak vector potential strength, U_p the ponderomotive energy, ω the laser frequency, N the total number of laser cycles and δ the carrier-envelope phase (CEP). We chose a $\delta = \pi/2$ CEP in order to avoid asymmetries in the angular distributions resulting from the asymmetry of the field. The laser field with the real and imaginary parts of the times of ionization is plotted in Fig. 2. These times are obtained by solving Eq. (13) considering an $I_p = 0.579$ a.u. ionization potential (corresponding to argon).

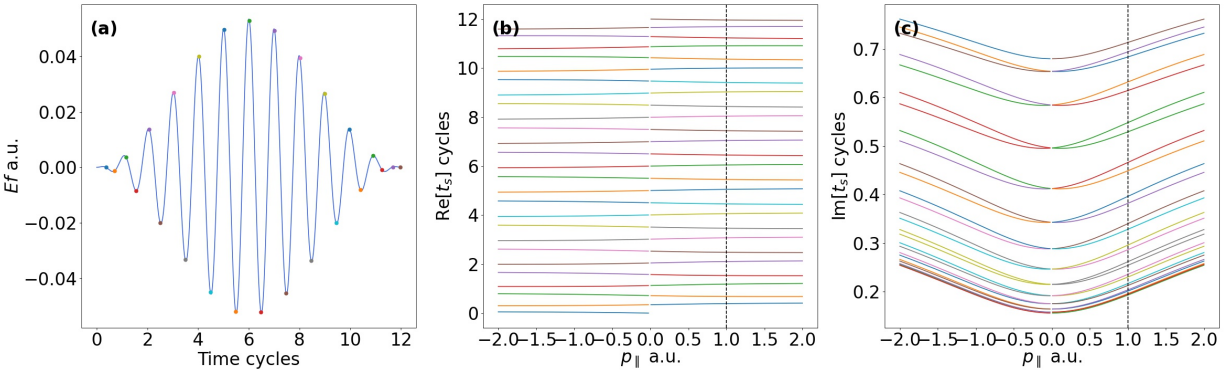

Figure 2: The 12-cycle electric field [panel (a)], real part of ionization times [panel (b)] and imaginary part of ionization times [panel (c)]. The electric field is related to the vector potential of Eq. (21) as $\mathbf{E}(t) = -\dot{\mathbf{A}}(t)$. The real part of the ionization times for $p_\parallel = 1$ a.u. are marked on the electric field of panel (a). The real and imaginary part of the ionization times are plotted vs the parallel momentum coordinate $p_\parallel$ for $\phi = 0$ and $\theta = \pi/3$. These times are obtained by solving Eq. (13) considering an $I_p = 0.579$ a.u. ionization potential. Laser field parameters: $U_p = 0.22$ a.u. (tunneling regime), $\omega = 0.057$ a.u. (corresponding to a 800 nm wavelength), $N = 12$ laser cycles and $\delta = \pi/2$. The associated laser peak intensity is $I = 10^{14}$ W/cm^2.

The prefactor clearly affects the momentum and transition amplitude distributions. Since $d(\mathbf{p}, t')$ can be seen as the Fourier transform of a hydrogen state $\psi_{n\ell m}(\mathbf{r})$ modified by the interaction $V(\hat{\mathbf{r}})$, its number of nodes is the same as for a hydrogen wave function ($n - \ell - 1$ radial nodes and $\ell - m$ angular nodes). Therefore, the presence of the prefactor means the appearance of radial and angular nodes depending on the initial state we are considering, as well as a shift in the peaks or a width change of the photoelectron momentum distribution. Nevertheless, this is only true in the velocity gauge, since in the length gauge most nodes vanish: all radial nodes vanish due to the absence of radial dependence, and the angular nodes are heavily transformed. Furthermore, the complex valued ionization times move the spherical harmonic away from a true node. The momentum distributions for different initial states are shown in Fig. 3. It can be seen that, for an initial symmetric state with respect to z, such as the states $|4d_{\pm1}\rangle$ or $|\chi_\rho^\pm\rangle$, the momentum distribution is also symmetric, while for an initial asymmetric state with respect to z, like the states $|\chi_c^\pm\rangle$ or $|\chi_c^\pm\rangle^*$, the momentum distribution is asymmetric.

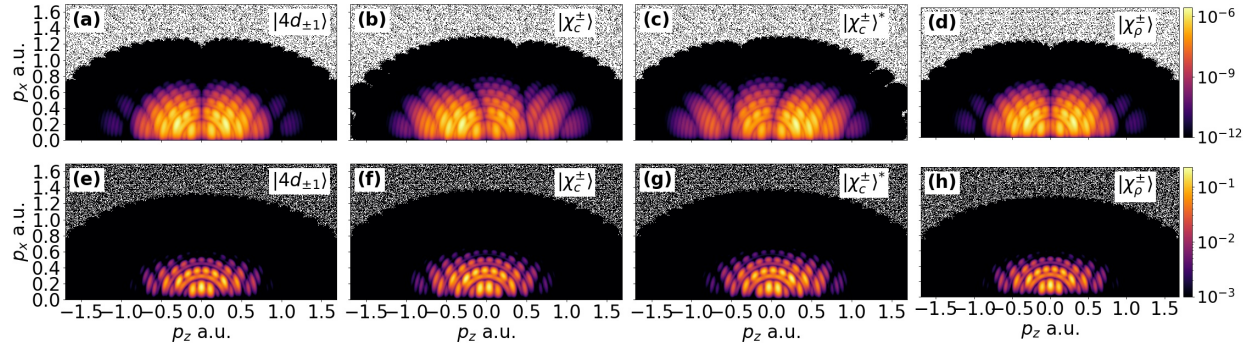

Figure 3: Momentum distributions in the velocity gauge (first row) and in the length gauge (second row) for different initial states. The units are arbitrary, normalized to its peak value, so the scale between gauges is different to highlight the relevant features. In the figure, Eq. (11) is being plotted as a function of the momentum coordinates p_x and p_z for $p_y = 0$. The laser parameters are the same as those used in Fig. 2.

In the length gauge, the hypergeometric function diverges and $d(\mathbf{p}, t_s) \to \infty$. Consequently, the prefactor has to be rewritten in a way to avoid the singularity. We have expanded the ${}_2F_1$ hypergeometric function and made a variable transformation. A modified saddle-point approximation has been applied, where the singularity has been transformed to an integral. Then, we have solved the different integrals and written the sum as a sum of ${}_3F_3$ hypergeometric functions, getting the expression for the prefactor without divergences (see Appendix A for the derivation).

The OAM distributions are numerically computed, using the saddle point approximation to compute the plane-wave transition amplitude of Eq. (11) and then performing the numerical computation of the ϕ integral of Eq. (16).

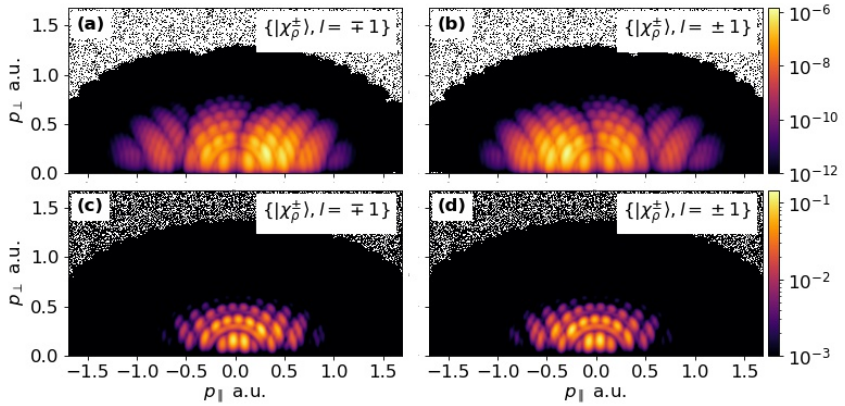

Figure 4: OAM distributions in the velocity gauge (first row) and in the length gauge (second row) for different initial states and OAM l values. As in Fig. 3, the units are arbitrary, normalized to its peak value. The distributions fulfil $M_{\pm1}(\chi_\rho^\pm) = M_{\pm1}(\chi_c^\pm)$ and $M_{\mp1}(\chi_\rho^\pm) = M_{\mp1}(\chi_c^{\pm *})$. Besides, the OAM distributions for the states $|4d_1\rangle$ and $|4f_1\rangle$ are symmetric with respect to $p_\parallel$. In the figure, Eq. (16) is being plotted vs the perpendicular $p_\perp$ and parallel $p_\parallel$ momentum coordinates. The laser parameters are the same as those used in Fig. 2.

When considering different initial states in the transition amplitude, we see that only the OAM distributions $l = m$ are populated (see Fig. 4), due to the conservation law stated in [18]. Therefore, for a hydrogen state $|n\ell_m\rangle$ or the $|\chi_c^\pm\rangle$ state (constituted by a superposition of two hydrogen states with the same m value), the photoelectron has an OAM value $l = m$. On the other hand, when considering a chiral initial state, such as the enantiomers $|\chi_\rho^\pm\rangle$ (constituted by superpositions of $m = -1$ and $m = +1$ hydrogen states), the electron ionizes with OAMs $l = \pm 1$. This can be seen analytically. For a field linearly polarized along z, the action of Eq. (16) has no ϕ dependence and

$$M_l(p_\parallel, p_\perp) \propto \int d\phi\, e^{-il\phi} M(\mathbf{p}) \propto \sum_m \delta_{m,l} \int dt' V_m(\mathbf{p}, t') e^{iS(\mathbf{p},t')} = \int dt' V_l(\mathbf{p}, t') e^{iS(\mathbf{p},t')}, \quad (22)$$

where V is related to the prefactor as $d(\mathbf{p}, t') = \sum_m e^{im\phi} V_m(\mathbf{p}, t')$. Therefore, the $m = \pm 1$ parts of the chiral state are picked out separately, being each part an asymmetric side of the chiral state, while the OAM $l = 0$ is suppressed. In other words, $M_{\pm1}(\chi_\rho^\pm) = M_{\pm1}(\chi_c^\pm)$ and $M_{\mp1}(\chi_\rho^\pm) = M_{\mp1}(\chi_c^{\pm *})$, where $M_l(\psi)$ denotes the transition amplitude $M_l(p_\parallel, p_\perp)$ for an initial state $|\psi\rangle$, where the momentum observables are dropped for simplicity.

Furthermore, we see that $M_{\pm1}(\chi_\rho^+) = M_{\mp1}(\chi_\rho^-)$, and we observe opposite asymmetries along $p_\parallel$ for opposite enantiomers $|\chi_\rho^+\rangle$ and $|\chi_\rho^-\rangle$. We call this new phenomenon photoelectron vortex dichroism (PEVD), an asymmetry in the OAM-resolved photoelectron angular distribution that allows us to distinguish between opposite enantiomers and, unlike PECD, it occurs for linear polarized fields.

Although both gauges show the same behavior, PEVD is not easy to see in the length gauge. Consequently, we have plotted the θ integral of the positive ($p_\parallel > 0$) and negative ($p_\parallel < 0$) hemispheres

of the OAM distributions in the length gauge in Fig. 5. A single hydrogen state shows a perfectly symmetric distribution, while the chiral states show the characteristic asymmetry between opposite enantiomers, as expected.

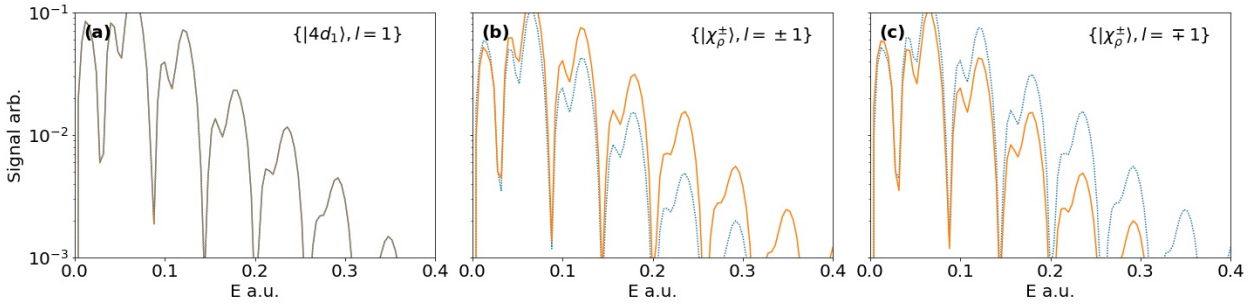

Figure 5: OAM distributions in the length gauge integrated over the positive (blue dashed lines) and negative hemispheres (orange solid lines) for different initial states and OAM l values. The integrals are plotted vs. the photoelectron energy, and the laser parameters are the same as those used in Fig. 2.

4. Conclusions

In this work, using an analytic formalism to produce chiral hydrogen states, we have investigated the strong field ionization of electrons by a linearly polarized laser field and how its OAM can be used to image molecular chirality.

Firstly, we have derived the transition amplitude of a ionizing electron in the SFA and the expression of the prefactor that takes into account the effects of the initial state on the photoelectron OAM, in the velocity and length gauges. The momentum and OAM distributions have been numerically computed for achiral and chiral hydrogen wave functions as initial states.

It has been seen that a photoelectron ionizing from a single hydrogen state has an OAM value equal to the magnetic quantum number of the initial state. Nevertheless, for a chiral hydrogen state, the electron ionizes with two OAM values due to the superposition of states with two different magnetic quantum numbers of the chiral state. Furthermore, it has been observed that the OAM distributions between the two enantiomers are asymmetric in the direction of the electric field. This phenomenon, which we have called photoelectron vortex dichroism, can be used to probe molecular chirality and distinguish enantiomers experimentally.

Further research could include calculations and comparisons with other methods, calculations on real molecules, orientation averaging, universality of the effect or the design of an experimental setup that would allow such measurements.

Acknowledgments

I would like to thank my supervisors, Dr. Andrew Maxwell, Dr. Andrés Ordoñez and Prof. Dr. Maciej Lewenstein, for their assistance and extremely helpful advice during all the project.

Also to my family, for their unconditional support on my path through the Physics world.

Appendix A. Derivation of the prefactor in the length gauge.

For simplicity, we write the prefactor as

$$d(\mathbf{p}, t') = \alpha_{n\ell} Y_\ell^m(\theta, \phi) \sum_{k=0}^{n-\ell-1} \beta_{n\ell k} \tilde{\mathbf{p}}^\ell {}_2F_1(a, b; c; z), \tag{A.1}$$

where $\alpha_{n\ell} = (-i)^\ell \sqrt{\frac{(n-\ell-1)!}{2n(n+\ell)!}}$, $\beta_{n\ell k} = (-2)^k \frac{(n+\ell)!\left(\sqrt{2I_p}\right)^{-\frac{1}{2}-\ell}}{\Gamma\left(\frac{3}{2}+\ell\right)(n-\ell-k-1)!k!}$, $a = \frac{1}{2}(2+k+2\ell)$, $b = \frac{1}{2}(3+k+2\ell)$, $c = \frac{3}{2}+\ell$ and $z = -\frac{\tilde{\mathbf{p}}^2}{2I_p}$.

The ${}_2F_1(a,b;c;z)$ hypergeometric function can be written as

$$ {}_2F_1(a,b;c;z) = \frac{\Gamma(c)}{\Gamma(a)\Gamma(c-b)} \sum_{\nu=0}^{\infty} \frac{\Gamma(a+\nu)\Gamma(c-b+\nu)}{\Gamma(c+\nu)\nu!} (-1)^\nu (2I_p)^{\nu+a} \frac{1}{[\tilde{\mathbf{p}}^2+2I_p]^{\nu+a}}, \tag{A.2}$$

where we have expanded the function by its definition, ${}_2F_1(a,b;c;z) = \frac{\Gamma(c)}{\Gamma(a)\Gamma(b)} \sum_{s=0}^{\infty} \frac{\Gamma(a+s)\Gamma(b+s)}{\Gamma(c+s)s!} z^s$ and made the variable transformation $F(a,b;c;z) = (1-z)^{-a} F(a,c-b;c;\frac{z}{z-1})$.

By introducing the expression of the prefactor with the hypergeometric function of Eq. (A.2) into the plane-wave transition amplitude of Eq. (11), we get

$$ M(\mathbf{p}) = \sum_{k=0}^{n-\ell-1} \sum_{\nu=0}^{\infty} \underbrace{\int_{-\infty}^{+\infty} dt' \frac{1}{[\tilde{\mathbf{p}}^2+2I_p]^{\nu+a}} e^{iS(\mathbf{p},t')} \nu_{n\ell mk\nu}(\mathbf{p},t')}_{I_{sp}}, \tag{A.3}$$

where

$$ \nu_{n\ell mk\nu}(\mathbf{p},t') = \frac{\Gamma(c)}{\Gamma(a)\Gamma(c-b)} \frac{\Gamma(a+\nu)\Gamma(c-b+\nu)}{\Gamma(c+\nu)\nu!} (2I_p)^a \alpha_{n\ell} Y_\ell^m(\theta,\phi) \beta_{n\ell k} \tilde{\mathbf{p}}^{\ell+2\nu}. \tag{A.4}$$

However, when applying the saddle-point method to solve the integral I_{sp}, we still have a singularity. This can be solved by modifying the saddle-point answer [27]. In the vicinity of the saddle point t_s, $S'(t_s) = 0$, we have $S'(t) \approx S''(t_s)(t-t_s)$. Therefore, since $\tilde{\mathbf{p}}^2 + 2I_p = S'(t)$,

$$ I_{sp} = \frac{\nu_{n\ell mk\nu}(\mathbf{p},t_s)}{[S''(\mathbf{p},t_s)]^{\nu+a}} \underbrace{\int_{-\infty}^{+\infty} dt' \frac{1}{(t'-t_s)^{\nu+a}} e^{iS(\mathbf{p},t')}}_{I_2}. \tag{A.5}$$

To solve I_2, which has a singularity at $t' = t_s$, we can use the transformation

$$ \frac{1}{(x-x_0)^\eta} = \frac{1}{\Gamma(\eta)} \int_0^\infty d\xi\, \xi^{\eta-1} \exp\left[-\xi\,(x-x_0)\right], \tag{A.6}$$

which leads to

$$ I_2 = \frac{1}{\Gamma(\nu+a)} \int_0^\infty d\xi \int_{-\infty}^{+\infty} dt' \xi^{\nu+a-1} \exp\left[-\xi\,(t'-t_s) + iS(\mathbf{p},t')\right]. \tag{A.7}$$

Calculating the integral, we get

$$ I_2 = i^{\frac{\nu+a}{2}} \frac{\Gamma(\frac{\nu+a}{2})}{2\Gamma(\nu+a)} \sqrt{\frac{2\pi i}{S''(\mathbf{p},t_s)}} [2S''(\mathbf{p},t_s)]^{\frac{\nu+a}{2}} e^{iS(\mathbf{p},t_s)}, \tag{A.8}$$

so, as $I_{sp} = \nu_{n\ell mk\nu}(\mathbf{p},t_s)[S''(\mathbf{p},t_s)]^{-(\nu+a)} I_2$, Eq. (A.3) becomes

$$ M(\mathbf{p}) = \frac{1}{2} \sqrt{\frac{2\pi i}{S''(\mathbf{p},t_s)}} e^{iS(\mathbf{p},t_s)} \tilde{d}(\mathbf{p},t_s), \tag{A.9}$$

with prefactor

$$ \tilde{d}(\mathbf{p},t_s) = \sum_{k=0}^{n-\ell-1} \sum_{\nu=0}^{\infty} \nu_{n\ell mk\nu}(\mathbf{p},t_s) i^{\frac{\nu+a}{2}} \frac{\Gamma(\frac{\nu+a}{2})}{\Gamma(\nu+a)} 2^{\frac{\nu+a}{2}} [S''(\mathbf{p},t_s)]^{-\frac{\nu+a}{2}}. \tag{A.10}$$

The second derivative of the action can be easily computed, getting

$$ S''(\mathbf{p},t_s) = -2\tilde{\mathbf{p}} E(t_s). \tag{A.11}$$

The prefactor can be separated in two sums by developing $\nu_{n\ell mk\nu}$:

$$\tilde{d}(\mathbf{p},t_s) = \sum_{k=0}^{n-\ell-1} \overbrace{\frac{\Gamma(c)}{\Gamma(a)\Gamma(c-b)}\alpha_{n\ell}Y_\ell^m(\theta,\phi)\beta_{n\ell k}(2I_p)^a\tilde{\mathbf{p}}^\ell(2i)^{a/2}[S''(\mathbf{p},t_s)]^{-a/2}}^{w_{n\ell k}(\tilde{\mathbf{p}},t_s)} \times \underbrace{\sum_{\nu=0}^{\infty}(2i)^{\nu/2}\frac{\Gamma(\frac{\nu+a}{2})\Gamma(c-b+\nu)}{\Gamma(c+\nu)\nu!}\tilde{\mathbf{p}}^{2\nu}[S''(\mathbf{p},t_s)]^{-\nu/2}}_{S_1}. \tag{A.12}$$

The S_1 can be solved by writting it as a combination of ${}_3F_3$ hypergeometric functions. Replacing S_1 and the other values in Eq. (A.12), we get the expression of the prefactor in the length gauge without divergences:

$$d(\mathbf{p},t_s) = (-i)^\ell\sqrt{\frac{(n-\ell-1)!}{2n\,(n+\ell)!}}Y_\ell^m(\theta_{\tilde{p}},\phi_{\tilde{p}})\sum_{k=0}^{n-\ell-1}\frac{(-1)^k(n+\ell)!2^k(2I_p)^{\frac{3}{4}+\frac{\ell}{2}+\frac{k}{2}}\tilde{\mathbf{p}}^\ell}{(n-\ell-k-1)!\;k!\;(i\tilde{\mathbf{p}}E(t_s))^{\frac{2+k+2\ell}{4}}} \times\frac{1}{\Gamma\left(\frac{3}{2}+\ell\right)\Gamma\left(\frac{2+k+2\ell}{2}\right)}\left[\Gamma\left(\frac{2+k+2\ell}{4}\right)F_1 - k\sqrt{\frac{4I_p^2}{i\tilde{\mathbf{p}}E(t_s)}}\frac{\Gamma(\frac{4+k+2\ell}{4})}{3+2\ell}F_2\right] \tag{A.13}$$

where $F_1 = {}_3F_3\left(\frac{2+k+2\ell}{4}, \frac{-k}{4}, \frac{2-k}{4}; \frac{1}{2}, \frac{5+2\ell}{4}, \frac{3+2\ell}{4}; \frac{I_p^2}{i\tilde{\mathbf{p}}E(t_s)}\right)$ and $F_2 = {}_3F_3\left(\frac{4+k+2\ell}{4}, \frac{2-k}{4}, \frac{4-k}{4}; \frac{3}{2}, \frac{5+2\ell}{4}, \frac{7+2\ell}{4}; \frac{I_p^2}{i\tilde{\mathbf{p}}E(t_s)}\right)$.

References

[1] Lloyd S, Babiker M, Thirunavukkarasu G and Yuan J 2017 *Reviews of Modern Physics* **89** 035004
[2] Bliokh K Y, Ivanov I P, Guzzinati G, Clark L, Van Boxem R, Béché A, Juchtmans R, Alonso M A, Schattschneider P, Nori F *et al.* 2017 *Physics Reports* **690** 1–70
[3] Asenjo-Garcia A and de Abajo F G 2014 *Physical review letters* **113** 066102
[4] Bonner W A 1995 *Origins of Life and Evolution of the Biosphere* **25** 175–190
[5] Francotte E, Lindner W, Mannhold R, Kubinyi H and Folkers G 2006 *Chirality in drug research* vol 33 (Wiley-VCH Weinheim)
[6] Ritchie B 1976 *Physical Review A* **13** 1411
[7] Böwering N, Lischke T, Schmidtke B, Müller N, Khalil T and Heinzmann U 2001 *Physical review letters* **86** 1187
[8] Beaulieu S, Ferré A, Géneaux R, Canonge R, Descamps D, Fabre B, Fedorov N, Légaré F, Petit S, Ruchon T *et al.* 2016 *New Journal of Physics* **18** 102002
[9] Krausz F and Ivanov M 2009 *Reviews of modern physics* **81** 163
[10] Ivanov M Y, Spanner M and Smirnova O 2005 *Journal of Modern Optics* **52** 165–184
[11] Amini K, Biegert J, Calegari F, Chacón A, Ciappina M F, Dauphin A, Efimov D K, de Morisson Faria C F, Giergiel K, Gniewek P *et al.* 2019 *Reports on Progress in Physics* **82** 116001
[12] Keldysh L 1965 *Sov. Phys. JETP* **20** 1307–1314
[13] Reiss H R 1980 *Physical Review A* **22** 1786
[14] Faisal F H 1973 *Journal of Physics B: Atomic and Molecular Physics* **6** L89
[15] Milošević D, Paulus G, Bauer D and Becker W 2006 *Journal of Physics B: Atomic, Molecular and Optical Physics* **39** R203
[16] Maxwell A S 2019 *Strong-Field Interference of Quantum Trajectories with Coulomb Distortion and Electron Correlation* Ph.D. thesis UCL (University College London)
[17] Maxwell A, Armstrong G, Ciappina M, Pisanty E, Kang Y, Brown A, Lewenstein M and de Morisson Faria C F 2021 *Faraday Discussions* **228** 394–412
[18] Kang Y, Pisanty E, Ciappina M, Lewenstein M, Faria C F d M and Maxwell A S 2021 *arXiv preprint arXiv:2102.07453*
[19] Tolstikhin O I and Morishita T 2019 *Physical Review A* **99** 063415
[20] Ordonez A F and Smirnova O 2019 *Physical Review A* **99** 043416
[21] Bauer D, Milošević D and Becker W 2005 *Physical Review A* **72** 023415
[22] Becker W, Grasbon F, Kopold R, Milošević D, Paulus G and Walther H 2002 *Advances in Atomic Molecular and Optical Physics* **48** 35–98
[23] Lewenstein M, Kulander K, Schafer K and Bucksbaum P 1995 *Physical Review A* **51** 1495
[24] Becker W, Lohr A, Kleber M and Lewenstein M 1997 *Physical Review A* **56** 645
[25] Smirnova O and Ivanov M 2013 Multielectron high harmonic generation: simple man on a complex plane (John Wiley & Sons)
[26] Maxwell A and de Morisson Faria C F 2015 *Physical Review A* **92** 023421
[27] Gribakin G and Kuchiev M Y 1997 *Physical Review A* **55** 3760